A&A 509, A70 (2010)
DOI: 10.1051/0004-6361/200913299

Astronomy & Astrophysics

The distance to the Andromeda galaxy from eclipsing binaries⋆,⋆⋆,⋆⋆⋆

F. Vilardell[1,2], I. Ribas[3], C. Jordi[2], E. L. Fitzpatrick[4], and E. F. Guinan[4]

[1] Departament de Física, Enginyeria de Sistemes i Teoria del Senyal, Universitat d'Alacant, Apartat 99, 03080 Alacant, Spain
e-mail: francesc.vilardell@ua.es
[2] Departament d'Astronomia i Meteorologia (ICC-IEEC), Universitat de Barcelona, c/ Martí i Franquès, 1, 08028 Barcelona, Spain
e-mail: carme.jordi@am.ub.es
[3] Institut de Ciències de l'Espai (CSIC-IEEC), Campus UAB, Facultat de Ciències, Torre C5, parell, 2a pl., 08193 Bellaterra, Spain
e-mail: iribas@ice.csic.es
[4] Department of Astronomy and Astrophysics, Villanova University, 800 Lancaster Avenue, Villanova, PA 19085, USA
e-mail: [edward.guinan;edward.fitzpatrick]@villanova.edu

Received 15 September 2009 / Accepted 6 November 2009

ABSTRACT

The cosmic distance scale largely depends on distance determinations to galaxies of the Local Group. In this sense, the Andromeda galaxy (M 31) is a key rung to better constrain the cosmic distance ladder. A project was started in 1999 to firmly establish a direct and accurate distance to M 31 using eclipsing binaries (EBs). After the determination of the first direct distance to M 31 from EBs, the second direct distance to an EB system is presented: M31V J00443610+4129194. Light and radial velocity curves were obtained and fitted to derive the masses and radii of the components. The acquired spectra were combined and disentangled to determine the temperature of the components. The analysis of the studied EB resulted in a distance determination to M 31 of $(m - M)_0 = 24.30 \pm 0.11$ mag. This result, when combined with the previous distance determination to M 31, results in a distance modulus of $(m - M)_0 = 24.36 \pm 0.08$ mag (744 ± 33 kpc), fully compatible with other distance determinations to M 31. With an error of only 4%, the obtained value firmly establishes the distance to this important galaxy and represents the fulfillment of the main goal of our project.

Key words. binaries: eclipsing – stars: fundamental parameters – stars: distances – distance scale – galaxies: individual: M 31

1. Introduction

Eclipsing binaries (EBs) have always been an important tool to test and determine the physical properties of stars (Popper 1967; Guinan 1993; Torres et al. 2009). They are composed of two stars which, when orbiting around each other, produce periodic eclipses. The great potential of EBs is that their orbital motion, inferred from the radial velocity curves, and the shape of the eclipses, obtained from the light curves, can be entirely explained by the gravitation laws and the geometry of the system (see Hilditch 2001, for details).

The direct determination of the radii of the components of EB systems made several authors (e.g., Lacy 1977; Giménez et al. 1994) suggest the possibility of using EBs for deriving distances. The only additional requirement to determine the absolute luminosity of an EB system and hence the distance is the surface brightness or, equivalently, the effective temperature of the components.

The potential of using EBs to derive distances encouraged several projects to obtain direct distance determinations either within the Milky Way (e.g., Munari et al. 2004), the Magellanic Clouds (e.g., Fitzpatrick et al. 2003, and references therein), or M 31/M 33 (DIRECT project, Kaluzny et al. 1998). In 1999, a new project was started to obtain a direct distance determination to the Andromeda galaxy (M 31) from EBs (Ribas & Jordi 2003; Ribas et al. 2004), providing the first direct distance determination in Ribas et al. (2005, hereafter Paper I).

The main interest for an accurate distance determination to M 31 lies in the potential of this galaxy to be a first-class distance calibrator (e.g., Clementini et al. 2001). The reasons for this are: (1) Contrary to the Magellanic Clouds, the distance to M 31 is large enough so that its geometry does not introduce any systematics in the final distance determination; (2) typically with a moderate reddening value ($E(B - V) = 0.16 \pm 0.01$, Massey et al. 1995), it is close enough to enable the individual identification of stars suitable for distance determination (such as EBs or Cepheids); (3) an Sb I–II giant spiral galaxy (like M 31) provides an appropriate local counterpart for the galaxies commonly used

⋆ Based on observations made with the Isaac Newton Telescope operated on the island of La Palma by the Isaac Newton Group in the Spanish Observatorio del Roque de los Muchachos of the Instituto de Astrofísica de Canarias.

⋆⋆ Based on observations obtained at the Gemini Observatory, which is operated by the Association of Universities for Research in Astronomy, Inc., under a cooperative agreement with the NSF on behalf of the Gemini partnership: the National Science Foundation (United States), the Science and Technology Facilities Council (United Kingdom), the National Research Council (Canada), CONICYT (Chile), the Australian Research Council (Australia), Ministério da Ciência e Tecnologia (Brazil) and Ministerio de Ciencia, Tecnología e Innovación Productiva (Argentina)

⋆⋆⋆ Original data are only available in electronic form at the CDS via anonymous ftp to cdsarc.u-strasbg.fr (130.79.128.5) or via http://cdsweb.u-strasbg.fr/cgi-bin/qcat?J/A+A/509/A70

Table 1. Log of spectroscopic observations and heliocentric radial velocity determinations (when available).

Date	Time [UT]	Exp. time [s]	S/N	HJD	Phase	Primary [km s^{-1}]	Secondary [km s^{-1}]
2004 Nov. 7	10:14	4100	22	2 453 316.931	0.272	–370.1 ± 8.2	143.5 ± 30.3
2004 Sep. 15	13:29	4100	11	2 453 264.066	0.467	...	...
2005 Feb. 12	5:39	3240	8	2 453 413.734	0.524	...	...
2004 Nov. 12	7:35	4100	15	2 453 321.820	0.659	14.3 ± 13.9	–414.1 ± 25.5
2004 Nov. 12	8:49	4100	16	2 453 321.872	0.684	57.3 ± 13.5	–448.2 ± 24.8
2004 Nov. 10	9:00	4100	24	2 453 319.879	0.711	30.6 ± 9.9	–455.5 ± 17.4
2004 Sep. 14	8:53	4100	20	2 453 262.874	0.885	...	...
2004 Sep. 12	9:45	4100	13	2 453 260.910	0.927	–69.7 ± 18.1	–309.2 ± 19.4
2004 Oct. 17	6:31	4100	14	2 453 295.776	0.946	–58.1 ± 24.2	–271.7 ± 22.9

for distance determination (e.g., Freedman et al. 2001); and (4) M 31 can also provide an absolute calibration of the Tully-Fisher relationship, enabling the calibration of the furthest distance determination methods. Therefore, the characteristics of this spiral galaxy make it an important step of the cosmic distance scale.

As mentioned above, our project already provided the first direct distance determination to M 31 (Paper I). However, the excellent dataset obtained (Sect. 2) allowed the determination of additional distances in order to further constrain the distance to M 31. Therefore, in the present work, we are presenting the second direct distance determination to M 31 from an EB system (Sects. 3–6). This result (which is the last one until further spectroscopic observations can be secured) enables us to engage in a critical discussion on the distance to M 31 (Sect. 7).

2. Observations

Photometric time series (in B and V passbands) were acquired with the Wide Field Camera at the 2.5 m Isaac Newton Telescope at La Palma (Spain). The field of observation covers $34' \times 34'$ at the north-eastern part of M 31. Around 260 images were obtained in each passband during five campaigns between 1999 and 2003. The Difference Image Analysis technique (DIA, Wozniak 2000) was used to perform the photometric data reduction (thoroughly explained in Vilardell et al. 2006, hereafter Paper II), providing light curves for more than 3964 variable stars with 437 being identified as EBs. In addition, the V photometric observations of the DIRECT project (Stanek et al. 1999) were also considered. Although the observations are somewhat noisier, they allowed us to extend the time baseline to 1996 and to ensure the consistency of our DIA photometry.

The EB sample was inspected to detect those targets more suitable for distance determination (see Paper II). A $5' \times 5'$ region containing five of the selected EBs was observed with the multi-object spectrograph (GMOS) at the Gemini-North telescope (program ID GN-2004B-Q-9). The instrumental setup was set to provide the highest possible resolution (R = 3744) using the slit width of $0\farcs5$ and the B1200_G5301 grism. The spectra cover the wavelength interval between 390 and 530 nm, with two gaps between 436.7–436.9 and 485.8–487.0 nm. A total of eight exposures were taken between September and November 2004 with an integration time of 4100 s each and an additional one with an exposure time of 3240 s in February 2005 (Table 1). The data reduction was performed with the Gemini IRAF package version 1.7, providing spectra with a S/N between 6 and 39 for the five selected EBs.

After careful analysis of the five EBs, two of the observed targets proved to be best-suited for obtaining a precise distance determination to M 31: M31V J00443799+4129236 and M31V J00443610+4129194. The first target was already analyzed in Paper I and the analysis of the second target is presented here. The three remaining EBs are unsuitable for distance determination. One of them is a single-line EB and the absolute properties of the stars cannot be obtained. Another EB is too faint for an accurate analysis of its spectra. The third one is a triple-line system, where the important contribution of the third light prevents a precise distance determination.

3. Radial velocities

The determination of radial velocities (RVs) was performed, as in the case of Paper I, with TODCOR (Zucker & Mazeh 1994) and the ATLAS9[1] and TLUSTY[2] (Lanz & Hubeny 2003, 2007) synthetic models. In this case, the best pair of synthetic spectra was determined with the following iterative approach. As a first step, the preliminary Wilson & Devinney (1971, hereafter W&D) fit (Sect. 4) was used to define an initial list with pairs of models having a temperature ratio, gravity ratio and rotational velocities compatible with the W&D parameters. All the model pairs in the initial list were then used to determine RVs, and a simple RV curve model was fitted to the obtained values. The free parameters in the fit were the semi-major axis (a), the systemic velocity (γ) and the mass ratio (q), while the period and reference time was fixed from the W&D solution. From all the derived solutions, the models having a lower dispersion around the fitted RV curve were selected, and all the neighboring models in the space of parameters were also attempted. The process was repeated until the local minimum was found, (i.e., none of the neighboring models has a scatter lower than the selected pair of models).

Since the resulting RVs depend, to some extent, on the W&D fit, the obtained values were used to find a new solution with the W&D (Sect. 4). The resulting W&D solution was then used to determine new RVs. The process was repeated until the pair of synthetic models providing the best fit was the same in two iterations. The final solution shown in Table 1 contains all the RVs (corrected to the heliocentric reference frame) that remained after the W&D fit (with 3σ clipping). Rejected observations shown in Fig. 1 were obtained during eclipses (one of them corresponds to the spectrum of February 2005 with a shorter exposure time).

The rejection of the observation at phase 0.885 can be explained neither by the proximity to the nodes (since other observations are obtained at larger phases) nor by a lower S/N of the observed spectrum. After some additional tests it was observed that the rejected observation could be recovered with different pairs of templates at the cost of losing other observations close

[1] Available at: http://kurucz.cfa.harvard.edu/
[2] Available at: http://nova.astro.umd.edu/

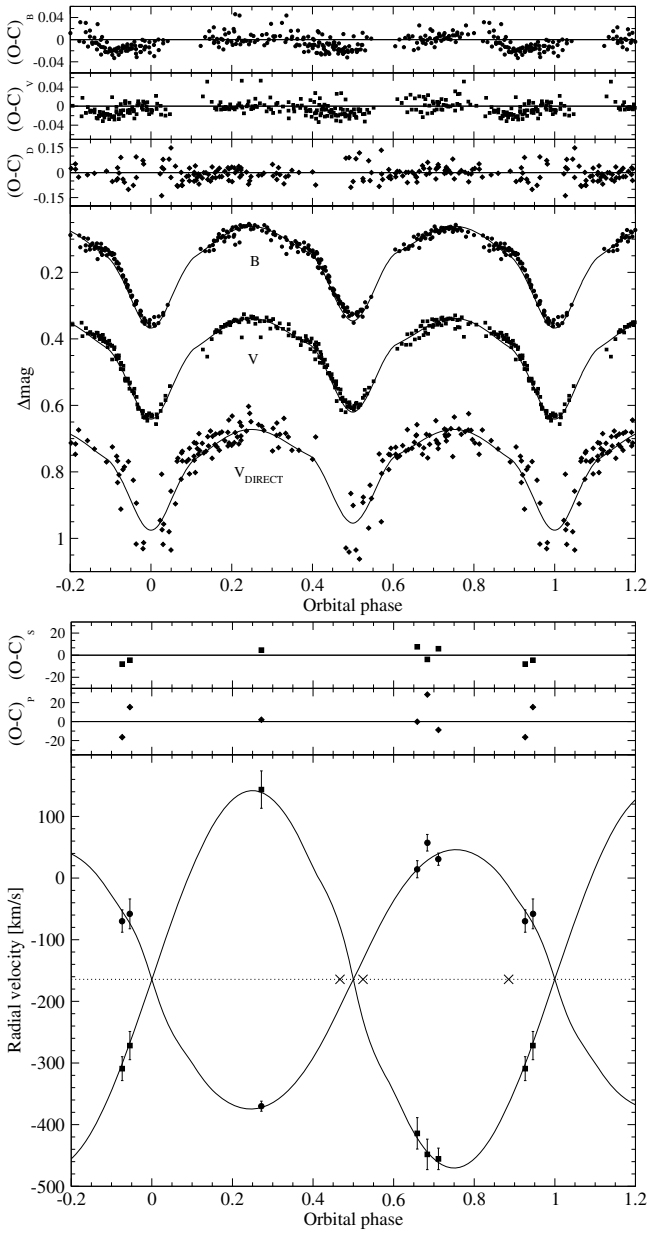

Fig. 1. Observations for M31V J00443610+4129194 and corresponding W&D fits. *Top*: light curve fits and corresponding residuals. *Bottom*: RV curve fits with RVs for the primary (circles) and secondary (squares) components with corresponding residuals. The phases of rejected RV observations are also indicated (crosses).

to the nodes and a larger dispersion of the fit. In all the different solutions attempted, the systemic velocities and semi-amplitudes were in perfect agreement with the solution presented here.

4. Mass and radius determination

The mass and radius determination was performed following the fitting procedure described in Paper I. Both semi-detached configurations (with either the primary or the secondary filling the Roche lobe) yield fits with the same residuals. The final configuration was adopted after the temperature determination analysis (Sect. 5). The spectra resulting from the disentangling indicate that the secondary is much fainter than the primary, while the assumption of the secondary filling its Roche lobe yields a flux ratio of $F_{V,S}/F_{V,P} = 0.85$. Therefore, a configuration where the primary (instead of the secondary) fills the Roche lobe was used in this case.

Table 2. Fundamental properties of M31V J00443610+4129194 derived from the analysis with W&D.

System properties		
$B_{\max}{}^a$ (mag)	19.832 ± 0.013	
$V_{\max}{}^a$ (mag)	19.948 ± 0.015	
P (days)	2.048644 ± 0.000007	
$t_{\min}$ (HJD)	2 452 908.694 ± 0.004	
i (deg)	69.9±1.6	
γ (km s^{-1})	–164 ± 5	
a ($R_\odot$)	22.6 ± 0.5	
$q \equiv \mathcal{M}_S/\mathcal{M}_P$	0.71 ± 0.04	
$T_{\rm eff,S}/T_{\rm eff,P}$	0.897 ± 0.019	
$F_{B,S}/F_{B,P}{}^a$	0.33 ± 0.03	
$F_{V,S}/F_{V,P}{}^a$	0.33 ± 0.03	
$F_{D,S}/F_{D,P}{}^a$	0.33 ± 0.05	
Component properties	Primary	Secondary
R ($R_\odot$)	9.2 ± 0.2	5.6 ± 0.4
$\mathcal{M}$ ($\mathcal{M}_\odot$)	21.7 ± 1.7	15.4 ± 1.2
$\log g$ (cgs)	3.85 ± 0.02	4.12 ± 0.05
K^b (km s^{-1})	210 ± 9	306 ± 11
$v_{\rm sync} \sin i$ (km s^{-1})	213 ± 6	131 ± 8

Notes. $^{(a)}$ Out of eclipse average: $\Delta\phi = [0.20{-}0.30, 0.70{-}0.80]$. $^{(b)}$ Including non-Keplerian corrections.

In order to ensure the viability of the adopted scenario and to rule out any other possible configurations, additional fits adopting a detached configuration were performed. The resulting parameters revealed that, depending on the initial value of the surface potential of the secondary component, either the primary or the secondary tended to fill their respective Roche lobes.

With the adopted configuration, the final rms residuals are 0.014 mag in B, 0.015 mag in V, and 0.047 mag in the DIRECT V light curve. The residuals of the RVs are 13 and 6 km s^{-1} for the primary and secondary components, respectively. The light and RV curves, with their respective fits superimposed, are shown in Fig. 1. The resulting best-fitting elements listed in Table 2 reveal two components with masses and radii of $\mathcal{M}_P = 21.7 \pm 1.7\ \mathcal{M}_\odot$, $R_P = 9.2 \pm 0.2\ R_\odot$ and $\mathcal{M}_S = 15.4 \pm 1.2\ \mathcal{M}_\odot$, $R_S = 5.6 \pm 0.4\ R_\odot$.

Light curves measured using DIA photometry require an accurate reference flux determination to avoid any bias in the scale of the light curves. Following the same procedure used for the EB in Paper I, several light-curve fits were performed with a variable third-light contribution (l_3). Again, the excellent agreement with DIRECT light curve and the convergence of the fits to $l_3 \sim 0$, ensures that the flux zero-point is correct and rules out any possible relevant blends with unresolved companions.

5. Temperature and distance determination

The last required ingredient to obtain a direct distance determination to M 31 is the temperature and line-of-sight absorption determination. Again, following the same procedure as in Paper I, we determined the temperature of the components by modeling their disentangled spectra. The spectral disentangling was performed with the KOREL program (Hadrava 1995) with all the required parameters fixed to the values determined from the W&D analysis (Sect. 4).

Considering the low S/N of the spectrum of the secondary, the fitting procedure was restricted to the primary component.

Table 3. Fundamental properties of M31V J00443610+4129194 and resulting distance determination, derived from the modeling of the optical spectrum of the primary component, using TLUSTY atmosphere models and the values of Table 2.

System properties		
M_V (mag)	–4.90 ± 0.08	
$E(B-V)$ (mag)	0.18 ± 0.02	
A_V (mag)	0.55 ± 0.08	
$(m-M)_0$ (mag)	24.30 ± 0.11	
Component properties	Primary	Secondary
$T_{\rm eff}$ (K)	33 600 ± 600	30 100 ± 900
$\log g$ (cgs)	3.86 ± 0.12	...
$v_{\rm rot} \sin i$ (km s^{-1})	189 ± 12	...
M_V (mag)	–4.59 ± 0.07	–3.38 ± 0.12
$(B-V)_0$ (mag)	–0.295 ± 0.002	–0.286 ± 0.004

The temperature ($T_{\rm eff}$), surface gravity ($\log g$) and rotational velocity ($v_{\rm rot} \sin i$) were fitted considering TLUSTY templates. Spectra with solar metallicity were adopted, since they were found to provide good fits to the observed spectrum. In addition, the EB analyzed in Paper I, only 29 arcsec from M31V J00443610+4129194, was found to have solar metallicity. The resulting values are listed in Table 3 together with the values of absolute luminosity (M_V) and intrinsic color ($(B-V)_0$). These values were computed by scaling the absolute magnitude in the models of Lejeune & Schaerer (2001) (for a given temperature and gravity) with the observed radii of the stars. When needed, the values resulting from the W&D fit were used (e.g., to determine the temperature of the secondary). This procedure is equivalent to the one used in Paper I, where instead of performing the synthetic photometry to obtain the surface fluxes, they were obtained from the models.

Finally, once the absolute magnitudes of the components are determined, the determination of the distance is straightforward. The resulting distance modulus to M31V J00443610+4129194 is $(m-M)_0 = 24.30 \pm 0.11$ mag or, equivalently, $d = 724 \pm 37$ kpc.

6. Comparison with stellar evolutionary models

The final step towards the characterization of M31V J00443610+4129194 is the comparison of the derived physical properties with stellar evolutionary models. The comparison has been mainly performed with the Geneva models of Lejeune & Schaerer (2001), with solar metallicity. Other models have been considered (Claret 2004) without any major differences to the derived conclusions. It is important to emphasize that the evolutionary tracks are built for isolated stars. In close binary systems, the evolution of both stars can be largely modified, with respect to their isolated evolutionary tracks, when one of the components fills the Roche lobe and mass transfer takes place (see, e.g., Vanbeveren 1993). In addition, due to the effects of mass loss in massive stars (due to stellar wind), the current derived masses of the components will be different from the masses at the Zero-Age Main Sequence (ZAMS). This is the reason why we initially fitted different evolutionary tracks in the mass-radius diagram to derive the mass of each component at the ZAMS ($\mathcal{M}_{P,\rm ZAMS} = 22.1\ M_\odot$, $\mathcal{M}_{S,\rm ZAMS} = 15.4\ M_\odot$).

Once the evolutionary tracks are adopted, the Hertzsprung-Russell (H-R) diagram can be studied. The location of the components on the H-R diagram (Fig. 3) reveals that both agree with their predicted evolutionary tracks. The derived properties seem characteristic of a detached system. However, as explained in Sect. 4, the W&D solutions supposing a detached configuration converge to solutions where either the primary or the secondary fill their respective Roche lobes. In addition, the disentangled spectra seem to favor the case where the primary is filling the Roche lobe, since it is much brighter than the secondary. All these observations can be explained supposing that M31V J00443610+4129194 is a pre-mass transfer EB system, where the primary component is *almost* filling its Roche lobe.

In a pre-mass transfer EB, both components are detached and should basically follow the evolution of single stars. This explains why the observed properties agree with the evolutionary tracks, since each component has evolved without any major interaction with the other component. This could also explain why the most massive component can be assumed to fill the Roche lobe. What is generally observed in semi-detached EBs is the Algol paradox, where the donor is the less massive component (as in the case of the EB in Paper I). The reason of this phenomenon (Paczyński 1971) is that when the donor is more massive than the companion, the mass transfer is very rapid, taking place on a thermal time scale ($\sim 10^5$ yr). But when the donor is the less massive companion, the mass transfer can last as long as the main-sequence life-time of the donor. The lack of any signature of intense mass transfer (such as an O'Connell effect in the light curves), combined with the short timescale of the process, renders a situation where the most massive component is filling the Roche lobe unlikely. However, the time spent in a situation where the massive component can almost fill the Roche lobe has a typical timescale of ~0.5 Myr, which makes the situation more likely to be observed.

The close agreement of the observations with the theoretical models, apart from clarifying the evolutionary stage of M31V J00443610+4129194, also allowed the fitting of an isochrone, resulting in an estimated coeval age of 4.2 ± 0.4 Myr.

7. The distance to M 31

The two analyzed EBs can be used to provide a distance determination to the M 31 galaxy (Table 4). As mentioned in Paper I, the derived distances to each EB can be associated to the center of M 31, because the correction due to the location of the EB within the galaxy is negligible (~0.3%). Therefore, the two independently derived distances, in mutual agreement within their one sigma error bars, show that EBs can be used to derive precise and accurate distances to M 31.

The two double-line EBs have been combined to derive a weighted mean distance to M 31 of 744 ± 33 kpc or $(m-M)_0 = 24.36 \pm 0.08$ mag. This resulting distance relies on the modeling of two different EBs and, therefore, can be considered to be:

Direct. The distance determination from EBs does not rely on previous calibrations and, since it is derived using a one-step procedure, it can be considered direct. Therefore, a recalibration of the distance to other Local Group galaxies (such as LMC) or a variation on the zero-point of any standard candle (such as Cepheids) has no effect on the derived distance. Furthermore, any standard candle in M 31 can be calibrated using our derived distance.

Precise. The uncertainty on the derived distance modulus of 0.08 mag represents a distance determination with an error of only 4%, which is remarkable, given the faintness of the studied targets. Although other distance determinations to M 31 with

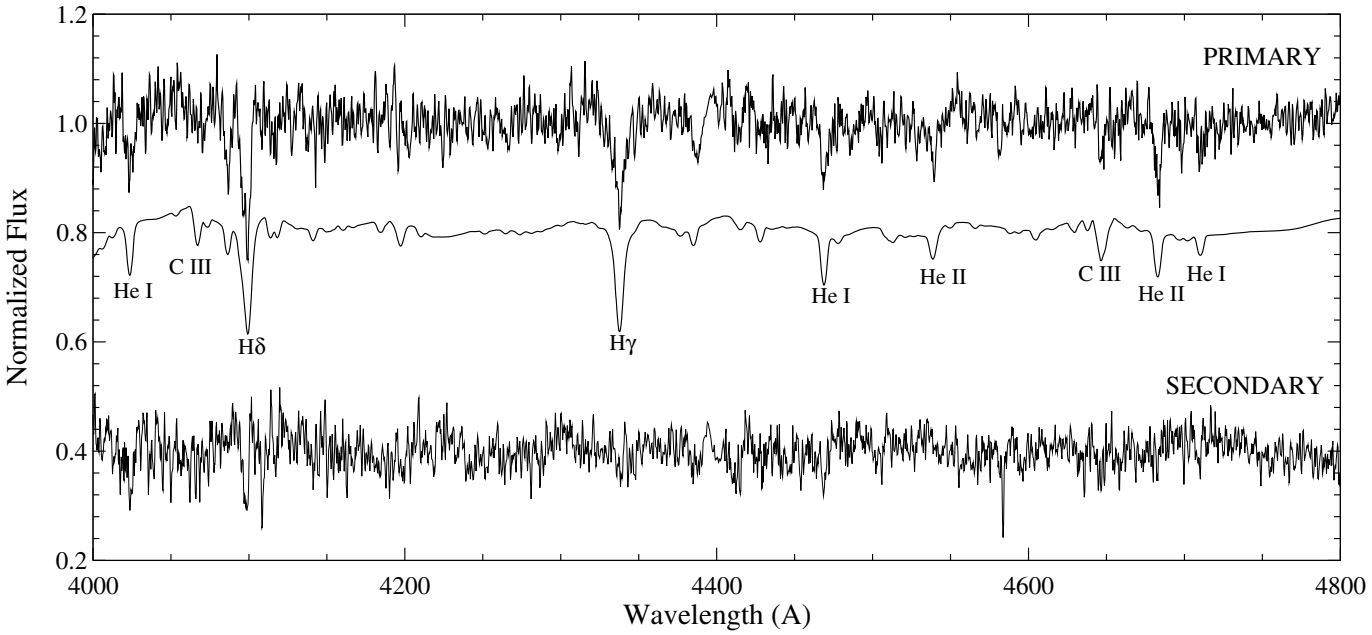

Fig. 2. Comparison of the individual disentangled spectrum for the primary component of M31V J00443610+4129194 (*above*) with the TLUSTY synthetic spectrum (*middle*). The bottom spectrum shows the noisy disentangled spectrum of the secondary component.

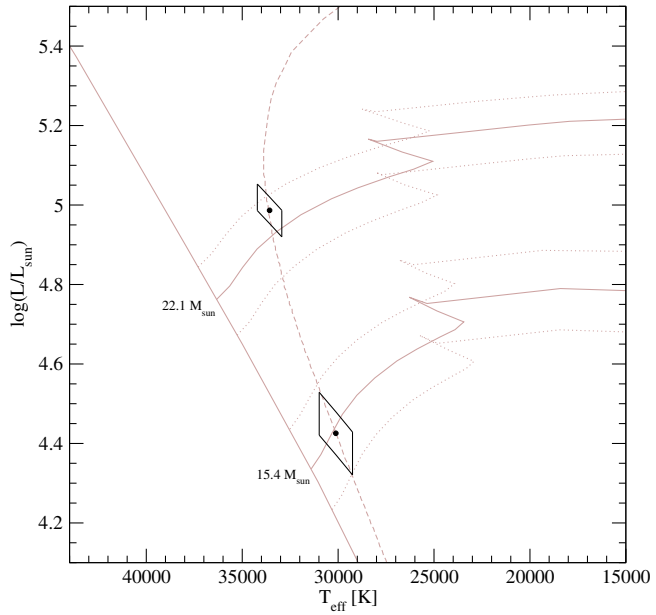

Fig. 3. Comparison of stellar evolutionary models with derived physical properties of M31V J00443610+4129194. Gray solid lines correspond to the ZAMS and the evolutionary tracks (ZAMS masses are indicated). The best fitting isochrone of 4.2 Myr is also shown (gray dashed line). Gray dotted lines denote the uncertainties in the derived masses. The skewed rectangular boxes correspond to 1σ error loci.

smaller errors have been reported (see a list in Paper II), most of these results do not consider the effect of systematics. In fact, the derived uncertainty is equal to the standard deviation resulting from the combination of the non-direct distance determinations in Paper II ($(m - M)_0 = 24.39 \pm 0.08$ mag) and, consequently, our derived distance is equally precise. The uncertainty in the derived distance could be improved with the analysis of additional EBs (already identified in the list of 24 EBs provided in Paper II), resulting in a distance determination to M 31 with a relative uncertainty of 2–3% and free of most systematic errors. This result would represent the most accurate and reliable distance determination to this important galaxy of the Local Group.

Accurate. One of the most important points when determining distances is the effect of possible systematics in the derived value. Contrary to other distance determinations, the uncertainty in our distance modulus includes most, if not all, the possible systematics. In particular, the possible sources of systematic errors and the corresponding considerations, can be summarized in the following points:

- Photometry. The photometry has been compared with other catalogs (Paper II) and checked to be well below 0.03 mag for the magnitude of the selected EBs.
- Assumed configuration in the modeling of the EBs. The configuration assumed is completely independent for each one of the two EBs used for distance determination and results in distances that agree within the uncertainties. In addition, M31V J00443799+4129236 shows clear evidence of being a semi-detached EB (O'Connell effect, no eccentricity, etc.) and M31V J00443610+4129194 has been thoroughly tested for any other possible configuration, with none of them being capable to reproduce the observations.
  It has traditionally been argued that detached EBs are the only systems capable to provide accurate distances. The most common reason is that non-detached EBs are affected by the proximity of the components, introducing distortions and reflection effects. But the proximity of the components can properly be taken into account by current modeling algorithms (such as W&D). In addition, the fact that one of the components fills the Roche lobe decreases the number of free parameters and greatly improves the stability of the solution (Wyithe & Wilson 2002). On the other hand, there are some other effects which are missing in detached EBs, that could introduce some systematics in the solutions (e.g., hot spots, circumstellar disks, etc.). In any case, these effects can be observed from the acquired data and properly modeled when they have a mild effect on photometry. A clear

Table 4. Distance determinations to M 31 from EBs.

EB system	V [mag]	M_V [mag]	A_V [mag]	$(m-M)_0$ [mag]	Distance [kpc]
M31V J00443799+4129236	19.27±0.02	–5.77 ± 0.06	0.60 ± 0.10	24.44 ± 0.12	772 ± 44
M31V J00443610+4129194	19.948±0.015	–4.90 ± 0.08	0.55 ± 0.08	24.30 ± 0.11	724 ± 37
Weighted mean	...	...	...	24.36 ± 0.08	744 ± 33

example of these effects is the presence of the O'Connell effect in M31V J00443799+4129236. The modeling we performed, with the introduction of a hot spot, enabled us to use M31V J00443799+4129236 for distance determination. Therefore, using semi-detached EBs reduces the number of free parameters, at the cost of having to account for some other effects that, when properly considered, should introduce no systematic error in the derived distances.

– Radial velocities. Several aspects have been considered with respect to the radial velocity determinations. TODCOR is a well-tested program which has been checked to introduce some systematics only for spectra with a narrow wavelength coverage (Torres & Ribas 2002), which is not our case. Moreover, the possible systematics introduced by the use of Balmer lines (that can be affected by stellar winds) is compensated with the incorporation of He lines. In addition, the stellar wind would introduce a bias mainly in the systemic velocity, which has no impact on the final distance determination. In any case, the derived systemic velocity ($\gamma = 164 \pm 5$ km s^{-1}) is in excellent agreement with the galactic rotation curve of M 31 (see, e.g., Brinks & Shane 1984, where the studied EB is at $(X, Y) \simeq (23'.3N, 8'.4E)$) and is very similar to the systemic velocity of the neighboring EB studied in Paper I ($\gamma = 173 \pm 4$ km s^{-1}). Which means that the effect of any systematics on the derived radial velocities can be considered to be negligible.
– Stellar atmosphere models used to determine the surface flux. This is probably the major source of systematic errors. In order to transform the derived temperatures and gravities to surface fluxes, the synthetic spectra are convolved with filter responses and are converted to absolute magnitudes and colors using a series of calibrations (see Lejeune & Schaerer 2001, for a description of the transformations applied). The accuracy of these transformations is usually defined within a few hundredths of magnitude (see Bessell et al. 1998, for various determinations of the bolometric corrections for the Sun and the colors of Vega, and Flower 1996, for the dispersion on the bolometric correction for hot stars). Consequently, we expect such systematic error to be no larger than a few per cent in flux, having an effect below 0.06 mag in the distance modulus.
– Line-of-sight absorption. The determination of the line-of-sight absorption benefits from the weak temperature dependence of $(B-V)_0$ above ~30 000 K to obtain an $E(B-V)$ value. Therefore, the main source of uncertainty at optical wavelengths is the determination of the total-to-selective extinction ratio ($\mathcal{R}_V$). The value of $\mathcal{R}_V$ has already been considered to have an uncertainty of 10% and larger variations are unlikely, as seen from previous statistical analysis (Fitzpatrick & Massa 2007). The large uncertainty in the value of $\mathcal{R}_V$ increases the line-of-sight absorption error. In fact, uncertainty in the extinction represents ~50% of the total error in the distance determination. So, any further improvements that reduce the uncertainty in the line-of-sight absorption could potentially improve the distance determinations presented here.

The precision and accuracy on the derived distance to M 31 enables us to draw a detailed comparison to previous results. The derived distance modulus completely agrees with the mean value obtained from the combination of non-direct distance determinations in Paper II. In fact, *all* the 18 distances reported agree with the EB value within 2σ and prove that the different distance indicators are all rather well calibrated within their error bars.

During the course of our project, Cepheids have also been used to determine a distance to M 31 (Vilardell et al. 2007). The derived distance modulus of $(m-M)_0 = 24.32 \pm 0.12$ mag represents an additional distance determination to M 31 that is fully compatible with the EB value. The consistency of this result is particularly valuable, because an EB distance to LMC has been used as reference. Therefore, the Cepheid distance modulus proves that the EB distances to LMC and to M 31 are fully compatible, tightening the extragalactic distance scale. In fact, Cepheids have proved to be extremely useful and robust to determine distances to LMC using as reference direct distance determinations to other galaxies. Macri et al. (2006) used the Cepheids in NGC 4258, which has a direct maser-based distance (Herrnstein et al. 1999), to determine a distance modulus to LMC that is almost identical to the EB value. It follows that the derived distances using EBs are not only fully compatible among themselves, but also with other direct distance determination methods.

An exception to the general agreement is the distance determination to M 33 with one EB system (Bonanos et al. 2006). The derived distance modulus is 0.3 mag larger that the Cepheid distance determination of Freedman et al. (2001), implying a distance to LMC that is incompatible with the remaining distance determinations. Even a maser-based distance to M 33 was obtained favoring the short distance to M 33 (Brunthaler et al. 2005), the associated uncertainty is too large for a firm establishment of the distance. Undoubtedly, additional distance determinations to M 33 with EBs will be crucial to solve the discrepancy.

EBs have proved to be excellent distance markers and are arguably the best method to provide direct distances for all the galaxies in the Local Group. In addition, the large number of distance indicators observed in M 31 strengthens the importance of this galaxy as the main calibrator for extragalactic distance determinations. In fact, all the distance indicators used to determine a distance to LMC (Gibson 2000) can be used in principle in M 31. Furthermore, at least two other distance determination methods can be used in M 31 (planetary nebulae luminosity function and Tully-Fisher relationship). Therefore, after the direct distance obtained with EBs, M 31 may be the best extragalactic benchmark for distance determinations.

Acknowledgements. This program was supported by grant AYA2006-15623-C02-01/02 of the Spanish Ministerio de Ciencia e Innovación (MICINN). F.V. acknowledges support from MICINN through a Consolider-GTC (CSD-2006-00070) fellowship.

References

Bessell, M. S., Castelli, F., & Plez, B. 1998, A&A, 333, 231
Bonanos, A. Z., Stanek, K. Z., Kudritzki, R. P., et al. 2006, ApJ, 652, 313
Brinks, E., & Shane, W. W. 1984, A&AS, 55, 179
Brunthaler, A., Reid, M. J., Falcke, H., Greenhill, L. J., & Henkel, C. 2005, Science, 307, 1440
Claret, A. 2004, A&A, 424, 919
Clementini, G., Federici, L., Corsi, C., et al. 2001, ApJ, 559, L109
Fitzpatrick, E. L., & Massa, D. 2007, ApJ, 663, 320
Fitzpatrick, E. L., Ribas, I., Guinan, E. F., Maloney, F. P., & Claret, A. 2003, ApJ, 587, 685
Flower, P. J. 1996, ApJ, 469, 355
Freedman, W. L., Madore, B. F., Gibson, B. K., et al. 2001, ApJ, 553, 47
Gibson, B. K. 2000, Mem. Soc. Astron. Ital., 71, 693
Giménez, A., Clausen, J. V., Guinan, E. F., et al. 1994, Experimental Astronomy, 5, 181
Guinan, E. F. 1993, in New Frontiers in Binary Star Research, ed. K.-C. Leung, & I.-S. Nha, ASP Conf. Ser., 38, 1
Hadrava, P. 1995, A&AS, 114, 393
Herrnstein, J. R., Moran, J. M., Greenhill, L. J., et al. 1999, Nature, 400, 539
Hilditch, R. W. 2001, An Introduction to Close Binary Stars (UK, Cambridge: Cambridge University Press)
Kaluzny, J., Stanek, K. Z., Krockenberger, M., et al. 1998, AJ, 115, 1016
Lacy, C. H. 1977, ApJ, 213, 458
Lanz, T., & Hubeny, I. 2003, ApJS, 146, 417
Lanz, T., & Hubeny, I. 2007, ApJS, 169, 83
Lejeune, T., & Schaerer, D. 2001, A&A, 366, 538
Macri, L. M., Stanek, K. Z., Bersier, D., Greenhill, L. J., & Reid, M. J. 2006, ApJ, 652, 1133
Massey, P., Armandroff, T. E., Pyke, R., Patel, K., & Wilson, C. D. 1995, AJ, 110, 2715
Munari, U., Dallaporta, S., Siviero, A., et al. 2004, A&A, 418, L31
Paczyński, B. 1971, ARA&A, 9, 183
Popper, D. M. 1967, ARA&A, 5, 85
Ribas, I., & Jordi, C. 2003, in Rev. Mex. Astron. Astrofis. Conf. Ser., 150
Ribas, I., Jordi, C., Vilardell, F., Giménez, Á., & Guinan, E. F. 2004, New Astron. Rev., 48, 755
Ribas, I., Jordi, C., Vilardell, F., et al. 2005, ApJ, 635, L37 (Paper I)
Stanek, K. Z., Kaluzny, J., Krockenberger, M., et al. 1999, AJ, 117, 2810
Torres, G., & Ribas, I. 2002, ApJ, 567, 1140
Torres, G., Andersen, J., & Giménez, 2009, A&ARv, 13
Vanbeveren, D. 1993, Space Sci. Rev., 66, 327
Vilardell, F., Ribas, I., & Jordi, C. 2006, A&A, 459, 321 (Paper II)
Vilardell, F., Jordi, C., & Ribas, I. 2007, A&A, 473, 847
Wilson, R. E., & Devinney, E. J. 1971, ApJ, 166, 605
Wozniak, P. R. 2000, Acta Astron., 50, 421
Wyithe, J. S. B., & Wilson, R. E. 2002, ApJ, 571, 293
Zucker, S., & Mazeh, T. 1994, ApJ, 420, 806